Depth distribution of luminescent Si nanocrystals in Si implanted SiO_2 films on Si

M. L. Brongersma[a] and A. Polman
FOM Institute for Atomic and Molecular Physics, Kruislaan 407, 1098 SJ Amsterdam, The Netherlands

K. S. Min and H. A. Atwater
Thomas J. Watson Laboratory of Applied Physics, California Institute of Technology, California 91125

(Received 11 December 1998; accepted for publication 6 April 1999)

Depth-resolved measurements of the photoluminescence of Si implanted and annealed SiO_2 films on Si have been performed to determine the depth distribution of luminescent Si nanocrystals. Si nanocrystals with diameters ranging from ~2 to 5 nm were formed by implantation of 35 keV Si ions into a 110-nm-thick thermally grown SiO_2 film on Si(100) at a fluence of 6×10^{16} Si/cm^2, followed by a thermal anneal at 1100 °C for 10 min. The photoluminescence spectrum is broad, peaks at $\lambda=790$ nm, and contains contributions from both recombination of quantum confined excitons in the nanocrystals and ion-implantation-induced defects. By chemical etching through the SiO_2 film in steps and analyzing the changes in the photoluminescence spectrum after each etch step, the depth from which each of the two luminescence features originate is determined. The etch rate of the oxide, as derived from Rutherford backscattering spectrometry data, varies from 1.3 nm/s in the regions of small excess Si to 0.6 nm/s at the peak of the concentration profile (15 at. % excess Si). It is found that the defect luminescence originates from an ~15-nm-thick near-surface region. Large nanocrystals luminescing at long wavelengths ($\lambda=900$ nm) are mainly located in the center of the film, where the Si concentration is highest (48 at. %). This is corroborated by transmission electron microscopy that shows a high density of Si nanocrystals in the size range of 2–5 nm in the center of the film. The largest density of small luminescent nanocrystals ($\lambda=700$ nm), not detectable by electron microscopy is found near the SiO_2 surface and the SiO_2/Si interface. This is attributed to either the fact that the surface and the SiO_2/Si interface affect the Si nanocrystal nucleation kinetics in such a way that small nanocrystals are preferentially formed in these regions, or an optical interaction between nanocrystals of different sizes that quenches the luminescence of small nanocrystals in the center of the film. © *1999 American Institute of Physics.* [S0021-8979(99)00714-8]

I. INTRODUCTION

Quantum size effects in Si nanostructures can be exploited to fit their electrical and optical properties for use in novel electronic and optoelectronic devices.[1–4] Forming Si nanocrystals by means of Si ion implantation into SiO_2 followed by precipitation has been extensively studied[5–10] and SiO_2 has proven to be a robust matrix that provides good chemical and electrical passivation of the nanocrystals. Previously, we have demonstrated that SiO_2 films containing Si nanocrystals made by ion implantation show photoluminescence in the visible and near-infrared that can be attributed to two distinct sources.[8] One luminescence feature is due to ion-irradiation-induced defects and could be quenched by introducing H or D into the film. The other is attributed to radiative recombination of quantum-confined excitons in the Si nanocrystals. The photoluminescence (PL) spectra are broad due to the presence of a wide distribution of nanocrystal sizes, in agreement with quantum-confinement theories that predict an increase of the band gap as a function of decreasing size.[11,12] If the Si ion implantation is performed with a single-ion energy, it will yield a Gaussian concentration depth profile of excess Si. As the nucleation and growth rates of Si nanocrystals from a supersaturated solid solution are strongly dependent on the local degree of supersaturation, the average nanocrystal size is expected to be depth dependent.

For applications of these nanocrystal-doped layers, e.g., in light-emitting structures, single-electron memories, or optical storage devices, it is essential to have detailed information on the exact nanocrystal size distribution as a function of depth. High-resolution cross-section transmission electron microscopy (TEM) may be used to study Si nanocrystals with sizes down to 2 nm. However, due to the small Z contrast between Si and SiO_2, nanocrystals with smaller sizes cannot be detected with TEM. Furthermore, TEM only provides structural information and does not reveal whether specific nanocrystals are optically active. In this article, the depth distribution of luminescent nanoparticles is determined by analyzing changes in the PL spectrum as the SiO_2 film is etched in a layer-by-layer fashion. It is found that the luminescence at the long wavelength side of the spectrum (emitted by the largest nanocrystals) mainly originates from the center of the SiO_2 film, in agreement with TEM. Large con-

[a]Electronic mail: Brongersma@amolf.nl;http://www.amolf.nl/departments/optoelec

tributions from small luminescent nanocrystals (not detectable by TEM) are found near the surface and the SiO_2/Si interface. It was also found that the defect luminescence that is often found in Si implanted SiO_2 film originates from the near-surface region.

II. EXPERIMENTAL

A 110-nm-thick SiO_2 film grown by wet thermal oxidation of a lightly B-doped Si(100) wafer was implanted at room temperature with 35 keV Si ions at a fluence of 6×10^{16} Si/cm^2. The sample was subsequently annealed at 1100 °C for 10 min in a vacuum at a base pressure below 3×10^{-7}mbar to induce nucleation and growth of Si nanocrystals.[8] Bright-field cross-sectional TEM images of the film were made under slightly unfocused conditions to enhance the contrast between the Si nanocrsytals and the SiO_2 matrix. The SiO_2 film containing the nanocrystals was then etched off in a series of subsequent etch steps of 10 s each, using buffered hydrofluoric acid (HF) at room temperature.

Rutherford backscattering spectrometry (RBS) was used to determine the Si concentration depth profiles after each etch step. A 2 MeV He^+ beam was used at an angle of 4° off the sample normal and a scattering angle of 92°. The depth resolution was 10 nm. Room-temperature PL spectra were taken using excitation with the 514 nm line of an Ar-ion laser at a power density of ~10 mW/mm^2. The angle between the randomly polarized laser beam and the sample normal was 30°. The luminescence was detected by a grating spectrometer in combination with a thermoelectrically cooled Si charge coupled device (CCD) detector array. All spectra were corrected for the system response. PL decay measurements were made at 15 K after pumping to a steady state with a power density of ~0.2 mW/mm^2. The pump light was chopped with an acousto-optic modulator and the lifetime traces were taken with a GaAs photomultiplier in combination with a multichannel photon counting system. The time resolution of the system was 400 ns.

III. RESULTS AND DISCUSSION

A. Si concentration depth profile and etch rate

Figure 1 shows Si concentration depth profiles of the Si implanted and annealed SiO_2 film on Si after several etch times ranging from 0 to 120 s, as indicated in the figure. The depth profiles were derived from RBS spectra taking into account the depth dependent electronic energy loss calculated from the relative Si/SiO_2 concentrations using Braggs rule and assuming a volume averaged density of Si (ρ=2.32 g/cm^3) and SiO_2 (ρ=2.29 g/cm^3). The depth scales for the concentration profiles are each shifted so that the SiO_2/Si interface is located at the same depth for all samples. The concentration profile of the as-implanted (unannealed) film (not shown) is nearly identical to that of the annealed film. The spectrum before etching, indicated by 0, shows the Si concentration profile with a peak concentration of 48 at. % Si at a depth of ~45 nm below the sample surface. Near the surface the Si concentration is 33 at. %, corresponding to that of stoichiometric SiO_2. The location of the SiO_2/Si interface is located at a depth of ~112 nm. Note that the Si concentration depth profile in the SiO_2 film is not Gaussian shaped, as predicted by a Monte Carlo calculation (TRIM '97),[13] and shows a relatively high Si concentration (~42 at. %) near the SiO_2/Si interface. The asymmetric shape of the profile could be the result of sputtering during the Si implantation, which progressively reduces the thickness of the film. The total sputtered layer thickness was estimated to be ~10 nm.[13] The concentration profiles obtained after etching for 10, 20, 40, 60, 80, 100, and 120 s clearly demonstrate that etching for progressively longer times reduces the SiO_2 film thickness further and further until the Si substrate is reached after 120 s.

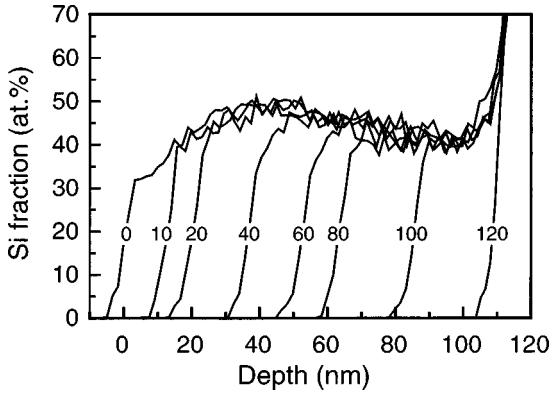

FIG. 1. Si concentration as a function of depth in an SiO_2 film that was implanted with 35 keV Si at a fluence of 6×10^{16} Si/ cm^2, and annealed at 1100 °C for 10 min to nucleate nanocrystals. Depth profiles after etching in buffered HF for times ranging from 0 to 120 s are also shown. Their depth scales are all shifted such that the SiO_2/Si interface is located at a depth of 112 nm. The profiles were calculated from RBS spectra taken with a 2 MeV He^+ beam at an angle of 4° off the sample normal and a scattering angle of 92°.

Figure 2 shows the etch depth as a function of time as obtained from the Si concentration profiles shown in Fig. 1. The drawn curve is a guide for the eye. The etch rate, as determined from the slope of this curve, varies from 1.3 nm/s in the regions with small excess Si to 0.6 nm/s at the peak of the Si concentration profile. An etch rate retardation has been observed before for Si-rich oxides with much higher Si supersaturation than in the present experiments.[14]

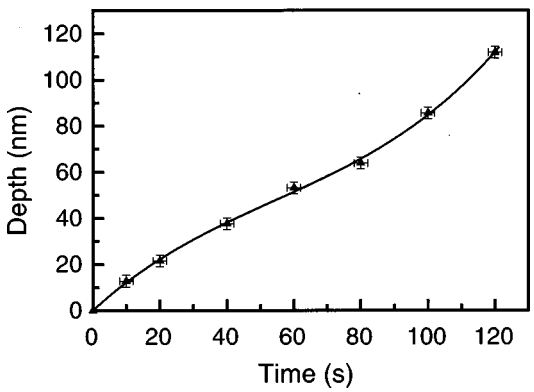

FIG. 2. Etch depth as a function of time as obtained from the Si concentration profiles shown in Fig. 1. The drawn curve serves as a guide to the eye.

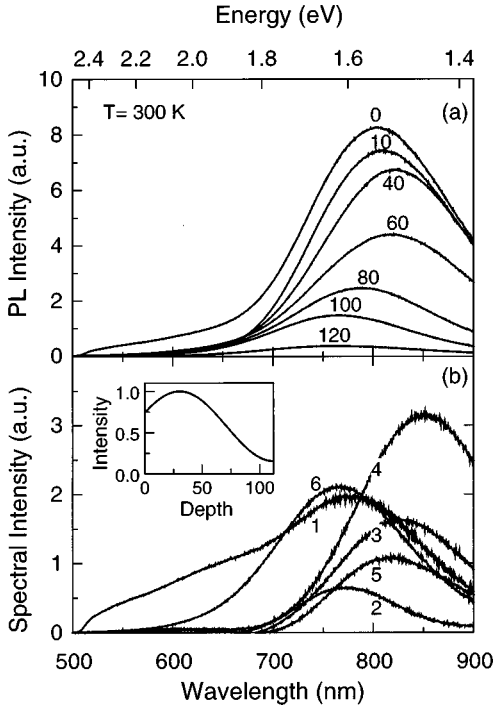

FIG. 3. (a) Room-temperature PL spectra ($\lambda_{pump}=514$ nm) obtained from a SiO_2 film containing Si nanocrystals, after etching in buffered HF for times ranging from 0 to 120 s. (b) Difference spectra obtained by subtracting the PL spectra for subsequent etch steps in (a), and corrected in such a way that the spectral intensity at a fixed wavelength is proportional to the average concentration of nanocrystals emitting at that wavelength. The inset shows the pump intensity profile as a function of depth in the SiO_2 film, resulting from internal reflections of the pump light at the SiO_2/Si interface and SiO_2/air interface.

B. Depth distribution of luminescent Si nanocrystals

Figure 3(a) shows room-temperature PL spectra obtained from the Si implanted and annealed SiO_2 film before and after etching several times up to 120 s. Before etching, the spectrum ranges from $\lambda=500$ nm to well beyond $\lambda=900$ nm. This corresponds to emission from nanocrystals with diameters of $\sim$2 nm and larger.[15] The spectrum peaks at $\lambda=790$ nm, corresponding to a nanocrystal diameter of $\sim$3–4 nm.[15] For increasing etch time, the overall PL intensity decreases continuously. Furthermore, the spectral shape and peak position also change upon each etch step. For example, after etching for 10–40 s, mostly components of the $\lambda=500$–800 nm part of the spectrum disappear, causing an apparent red shift of the peak position. For longer etch times, the $\lambda=800$–900 nm spectral region shows a decrease as well. A small luminescence signal remains after 120 s. This is attributed to the presence of luminescent nanocrystals left on the substrate after the oxide layer is completely etched off. Indeed, atomic-force microscopy shows the presence of such nanocrystals at the surface of the fully etched film.

Figure 4 shows two normalized luminescence decay traces at $\lambda=650$ nm, measured at 15 K before and after etching for 10 s, and plotted on a logarithmic intensity scale. The trace taken before etching clearly shows two components with substantially different lifetimes. This is in agreement with previously obtained results, that demonstrated the existence of two luminescence sources in SiO_2 films containing

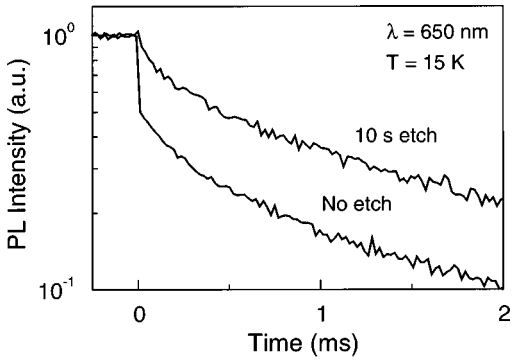

FIG. 4. Two luminescence decay traces taken at 15 K and 650 nm from the nanocrystals containing SiO_2 films before and after etching for 10 s in buffered HF, and plotted on a logarithmic intensity scale. The pump beam at 514 nm was switched off at time=0 ms.

Si nanocrystals made by ion implantation.[8] One broad luminescence feature peaking at $\lambda=600$ nm was shown to be related to ion-irradiation-induced defects and has a lifetime shorter than 400 ns. The other was attributed to radiative recombination of quantum-confined excitons in the Si nanocrystals with a $1/e$ decay time on the order of 1.0 ms at 15 K. After etching for 10 s, the short lifetime component disappears. It is therefore concluded that the defect luminescence originates from the first etched layer, an $\sim$15 nm thick near-surface region. This is corroborated by the data in Fig. 3(a), which show that the PL intensity around $\lambda=600$ nm, attributed to defect luminescence, completely disappears after etching for 10 s. The fact that these luminescent defects are located in the near-surface region indicates that they are either preferentially formed near or at the SiO_2 surface or in regions with a low Si supersaturation. PL lifetime measurements (not shown) indicate that the defect luminescence is negligible at wavelengths longer than 700 nm.

After etching off the top part of the film that contained most of the luminescent defects, the decrease in PL intensity that was observed for longer etch times must be due to the removal of luminescent nanocrystals. Since the luminescence wavelength depends on the size of the nanocrystals, removal of a particular size nanocrystal will result in a decrease of the PL intensity at a certain wavelength. For example, a decrease in intensity at the short (long) wavelength side of the spectrum indicates that a layer containing small (large) size nanocrystals was etched off. At each wavelength the concentration of luminescent nanocrystals as a function of depth, $n_\lambda(x)$, can then be calculated from the decrease in PL intensity observed after each etch step. In the calculation of $n_\lambda(x)$ from the different PL spectra, two correction factors should be taken into account. First, from the Si depth profiles in Fig. 1 it is clear that each step did not remove the same amount of material and this should be corrected. Second, it should be realized that due to internal reflections of the pump light at the SiO_2/air and the SiO_2/Si interface a standing light wave builds up in the SiO_2 film. This implies that nanocrystals located at different depths are not excited with the same intensity. A calculation of the pump intensity as a function of depth in the SiO_2 film before etching is shown as an inset in Fig. 3(b). Input parameters for this calculation are the SiO_2

film thickness of 112 nm and an average effective refractive index of the nanocrystal containing SiO_2 film of 1.65, as calculated by the Maxwell-Garnett theory.[16] The peak intensity is normalized to 1, and as seen in the inset the intensity varies by a factor 6.6 over the SiO_2 film thickness. For the determination of $n_\lambda(x)$, both the calculated shape of the pump intensity profile in the SiO_2 film and the changes that occur in this profile as the film gets thinner after each etch step were taken into account.

Figure 3(b) shows the corrected difference spectra of Fig. 3(a), numbered according to the layer that was etched off. For each etch step one can now clearly see in which part of the spectrum the luminescence decreases and whether small or large nanocrystals were removed. For example, the largest decrease in the PL intensity at wavelengths shorter than 700 nm occurs during the first (1) and last (6) etch step. This means that almost all the small luminescent nanoparticles are located near the SiO_2 film surface or close to the SiO_2/Si interface.

Figure 5(a) shows a histogram of the depth dependence of the concentration of nanocrystals luminescing at $\lambda=700$ nm, n_{700}, as obtained from the six difference spectra in Fig. 3(b). The distribution of the relatively large nanocrystals emitting at $\lambda=900$ nm is shown in Fig. 5(b). The highest concentration of these nanocrystals is found in the center of the film, where the excess Si concentration is highest. For comparison, Fig. 5(c) shows the excess Si concentration as a function of depth before etching, as obtained from Fig. 1. Figure 5(d) shows a bright-field cross-sectional TEM image of the film. Despite the weak Z contrast between the Si and SiO_2, it shows Si particles in the size range of 2–5 nm. As can be seen, the largest nanocrystals are mainly located near the center of the film, in agreement with the results obtained for n_{900} in Fig. 5(b). The TEM image does not show a high concentration of nanoparticles near the surface or near the Si/SiO_2 interface, in contrast to what the 700 nm data in Fig. 5(a) indicate. It may well be that the nanocrystals emitting at 700 nm are too small to be seen by TEM. Alternatively, it may be that their concentration is very low. Note that the relative scales of n_{700} and n_{900} may not be compared, as nanocrystals of different size have different optical excitation cross sections and luminescence efficiencies.

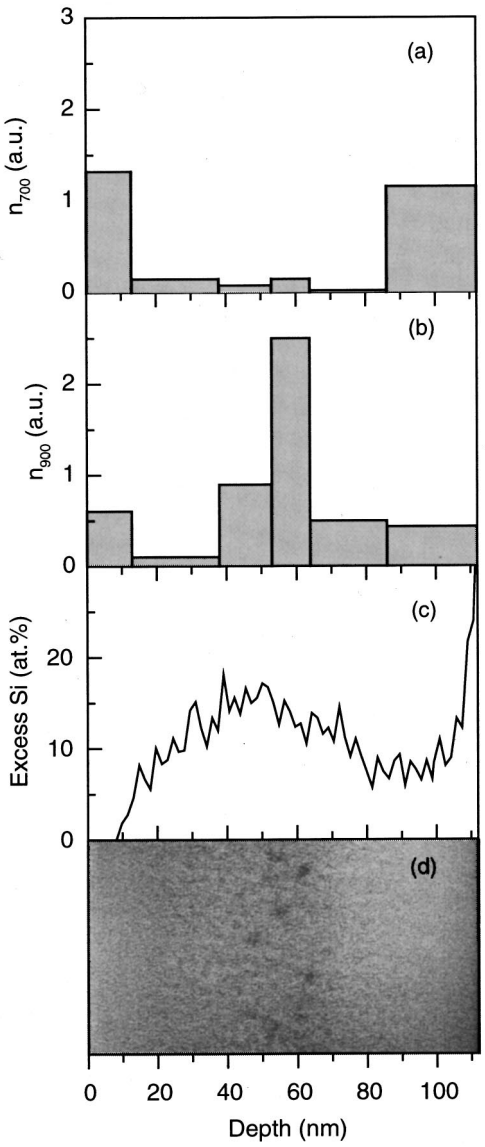

FIG. 5. Histogram of the depth dependence of the concentration of optically active Si nanocrystals, emitting at $\lambda=700$ nm (a) and $\lambda=900$ nm (b), obtained from the data in Fig. 3. (c) The concentration of excess Si in the SiO_2 film as calculated from Fig. 1. (d) Bright-field cross-sectional TEM image of the nanocrystal containing SiO_2 film that was made under slightly defocused conditions to enhance the contrast between the Si nanocrystals and the SiO_2 matrix.

The observation that the luminescence from small nanocrystals originates mainly from the near-surface region and the region near the Si/SiO_2 interface is very intriguing. It has important consequences for the engineering of Si nanocrystal size distributions in general. The origin of this peculiar distribution may be related to the nanocrystal size distribution itself, or to variations in the luminescence efficiency across the film, as will be discussed below.

From recent experiments it is known that the local average nanocrystal size for these annealing conditions increases with Si supersaturation,[17] in agreement with classical particle coarsening theory.[18] This would explain that small nanocrystals are only found in the region with low supersaturation, i.e., near the surface. However, this argument does not explain the high density of small nanocrystals near the SiO_2/Si interface as the supersaturation in that region is still quite high (8 at. %) [see Fig. 5(c)]. Alternatively, it is very likely that the surface and the SiO_2/Si interface both act as a sink for diffusing Si, thereby altering the local nanocrystal nucleation and growth kinetics such that relatively large amounts of small nanocrystals are formed. Indeed, such an effect has been observed for the case of Ge implanted SiO_2 films with a relatively high concentration of as-implanted Ge near the SiO_2/Si interface. For these films a narrow band of Ge nanocrystals was found close ($\sim$10 nm) to the Si/SiO_2 interface.[19] In the present experiments, the typical Si diffusion distance at 1100 °C, 10 min is a few nm,[14] so that strong effects on the nucleation kinetics can indeed be expected close to the two interfaces. In this way surfaces and interfaces may be used in the future to fit size distributions of Si nanocrystals in SiO_2.

An alternative explanation for the observation that luminescence of small nanocrystals is not found in the center of the film is related to an optical interaction between nanocrystals. At the high nanocrystal densities in the center of the film, excitation migration due to dipole–dipole interaction or charge exchange may take place.[20–24] In this process, migration will only take place from small nanocrystals (large band gap) to large nanocrystals (small band gap). As a result, luminescence from small nanocrystals would be quenched in the center of the film.

As an interesting corollary we note that the variation in PL emission intensity across the film is also affected by the variation of the local classical optical density of states over the thickness of the film, since it will influence the spontaneous emission rate of Si nanocrysals.[25] Mode calculations show that the density of states in each of the six etched layers in the film varies as a function of depth by at most a factor 4. It can be calculated that the net effect of the variation in the local density of states on the nanocrystal emission intensity is <3.2, depending on the internal nanocrystal quantum efficiency. This cannot explain the high luminescence yield from small nanocrystals close to the Si substrate compared to that in the center of the film.

IV. CONCLUSIONS

By studying the evolution of the PL spectrum of a SiO_2 film containing Si nanocrystals as the film is progressively etched off, depth resolved information is obtained on the location of all luminescence sources present in the film. It is found that the defect luminescence centered around $\lambda=600$ nm mainly originates from a $\sim$15 m-thick near-surface region. Large Si nanocrystals emitting at $\lambda=900$ nm are mainly located in the center of the oxide film, where the Si concentration is highest. This is in agreement with TEM that shows that the largest (4–5 nm diameter) nanocrystals are located in the center of the film. The luminescence from small nanocrystals, luminescing at $\lambda=700$ nm and shorter wavelengths, mainly originates from regions close to the SiO_2 film surface and the SiO_2/Si interface. This may be due to the fact that the surface and the interface affect the Si nanocrystal nucleation kinetics in such a way that small nanocrystals are preferentially formed. Alternatively, it may be that the luminescence of small Si nanocrystals is quenched in the center of the film, due to excitation migration from small nanocrystals to large ones. The results may be used to engineer the size distribution of Si nanocrystals for a variety of applications.

ACKNOWLEDGMENTS

This work is part of the research program of the ''Stichting voor Fundamenteel Onderzoek der Materie (FOM),'' which is financially supported by the ''Nederlandse Organisatie voor Wetenschappelijke Onderzoek (NWO),'' and the ESPRIT program of the European Community. Jan van der Elsken is acknowledged for discussions and Michiel de Dood is acknowledged for the calculation of optical mode densities.

[1] S. Tiwari, F. Rana, H. Hanafi, A. Hartstein, E. Crabbe, and K. Chan, Appl. Phys. Lett. **68**, 1377 (1996).
[2] K. D. Hirschman, L. Tsybeskov, S. D. Duttagupta, and P. M. Fauchet, Nature (London) **384**, 338 (1996).
[3] Y. Kanemitsu, Phys. Rep. **263**, 1 (1995).
[4] M. L. Brongersma, K. S. Min, E. Boer, T. Tambo, A. Polman, and H. A. Atwater, Mater. Res. Soc. Symp. Proc. **486**, (1998).
[5] T. Shimizu-Iwayama, M. Oshima, T. Niimi, S. Nakao, K. Saitoh, T. Fujita, and N. Itoh, J. Phys.: Condens. Matter **5**, 375 (1993).
[6] J. G. Zhu, C. W. White, J. D. Budai, S. P. Withrow, and Y. Chen, Mater. Res. Soc. Symp. Proc. **358**, 175 (1995).
[7] G. Ghislotti, B. Nielsen, P. Asoka-Kumar, K. G. Lynn, A. Gambhir, L. F. Di Mauro, and C. E. Bottani, J. Appl. Phys. **79**, 8660 (1996).
[8] K. S. Min, K. V. Shcheglov, C. M. Yang, H. A. Atwater, M. L. Brongersma, and A. Polman, Appl. Phys. Lett. **69**, 2033 (1996).
[9] J. Linnros, A. Galeckas, N. Lalic, and V. Grivickas, Thin Solid Films **297**, 167 (1997).
[10] L. Rebohle, L. Borany, R. A. Yankov, W. Skorupa, I. E. Tyschenko, H. Fröb, and K. Leo, Mater. Res. Soc. Symp. Proc. **486**, (1998).
[11] M. S. Hybertsen, Phys. Rev. Lett. **72**, 1514 (1994).
[12] C. Delerue, G. Allan, and M. Lannoo, Phys. Rev. B **48**, 11024 (1993).
[13] J. P. Biersack and L. J. Haggmark, Nucl. Instrum. Methods **174**, 257 (1980).
[14] *Quick Reference Manual for Si Integrated Circuit Technology*, edited by W. E. Beadle, J. C. C. Tsai, and R. D. Plummer (Wiley, New York, 1985).
[15] R. T. Collins, P. M. Fauchet, and M. A. Tischler, Phys. Today **1**, 24 (1997).
[16] J. C. Maxwell-Garnett, Philos. Trans. R. Soc. London **203**, 385 (1904).
[17] M. L. Brongersma, M. J. A. de Dood, K. S. Min, H. A. Atwater, and A. Polman (unpublished).
[18] L. A. Nesbit, Appl. Phys. Lett. **46**, 38 (1985).
[19] J. von Borany, R. Grötzschel, K. H. Heinig, W. Matz, B. Schmidt, and W. Skorupa, Appl. Phys. Lett. **71**, 3215 (1997).
[20] Th. Förster, in *Comparative Effects of Radiation*, edited by M. Burton, J. S. Kirby-Smith, and J. L. Magee (Wiley, New York, 1960), p. 301.
[21] D. L. Dexter, J. Chem. Phys. **21**, 836 (1953).
[22] C. R. Kagan, C. B. Murray, M. Nirmal, and M. G. Bawendi, Phys. Rev. Lett. **76**, 1517 (1996).
[23] J. C. Vial, A. Bsiesy, F. Gaspard, R. Herino, M. Ligeon, F. Muller, R. Romestain, and R. M. Macfarlane, Phys. Rev. B **45**, 14171 (1992).
[24] I. Mihalcescu, J. C. Vial, and R. Romestain, Phys. Rev. Lett. **80**, 3392 (1998).
[25] E. Snoeks, A. Lagendijk, and A. Polman, Phys. Rev. Lett. **74**, 2459 (1995).